On the Full and Global Accuracy of a Compact Third Order WENO Scheme: Part II

Oliver Kolb

Abstract Recently, we showed in (O. Kolb, *SIAM J. Numer. Anal.*, 52 (2014), pp. 2335–2355) for which parameter range the compact third order WENO reconstruction procedure introduced in (D. Levy, G. Puppo, and G. Russo, *SIAM J. Sci. Comput.*, 22 (2000), pp. 656–672) reaches the optimal order of accuracy (h^3 in the smooth case and h^2 near discontinuities). This is the case for the parameter choice $\varepsilon = Kh^q$ in the weight design with $q \leq 3$ and $pq \geq 2$, where $p \geq 1$ is the exponent used in the computation of the weights in the WENO scheme. While these theoretical results for the convergence rates of the WENO reconstruction procedure could also be validated in the numerical tests, the application within the semi-discrete central scheme of (A. Kurganov, and D. Levy, *SIAM J. Sci. Comput.*, 22 (2000), pp. 1461–1488) together with a third order TVD-Runge-Kutta scheme for the time integration did not yield a third order accurate scheme in total for $q > 2$. The aim of this follow-up paper is to explain this observation with further analytical and numerical results.

1 Introduction

We are interested in the numerical solution of hyperbolic conservation laws

$$\frac{\partial}{\partial t}u(x,t) + \frac{\partial}{\partial x}f(u(x,t)) = 0 \tag{1}$$

with given initial conditions $u(x,0) = u_0(x)$. One major difficulty arises here due to the fact that even for smooth initial data, the solutions of (the weak form of) (1) may contain discontinuities after finite time. At the same time, one is interested in resolving complex smooth solution structures with high order of accuracy. Based on the pioneering works [9, 15], the approach of so-called weighted essentially non-oscillatory (WENO) schemes allows the combination of high resolution with

O. Kolb (✉)
Department of Mathematics, University of Mannheim, A5,6 in 68131 Mannheim, Germany
e-mail: kolb@uni-mannheim.de

B. Karasözen et al. (eds.), *Numerical Mathematics and Advanced Applications ENUMATH 2015*, Lecture Notes in Computational Science and Engineering 112, DOI 10.1007/978-3-319-39929-4_6

a stable behaviour in the presence of discontinuities. The key ingredient of such schemes is a weighting of discretization stencils or reconstruction polynomials based on smoothness indicators.

As already noted in [11], WENO reconstructions may not attain the optimal order at critical points and meanwhile there are several fixes for that problem like [2–4, 6, 8, 10, 16–18]. Based on the smoothness indicator of [11], Aràndiga et al. recently proposed in [1] to choose the parameter ε, which occurs in the denominator within the weight design, proportional to the square of the mesh size, h^2. For the compact third order WENO (CTO-WENO) reconstruction procedure introduced in [14], we recently showed in [12] that it reaches the optimal order of accuracy (h^3 in the smooth case and h^2 near discontinuities) for the parameter choice $\varepsilon = Kh^q$ with $q \leq 3$ and $pq \geq 2$, where $p \geq 1$ is the exponent used in the computation of the weights in the WENO scheme. While these theoretical results for the convergence rates of the CTO-WENO reconstruction procedure could also be validated in the numerical tests, the application within the semi-discrete central scheme of [13] together with a third order TVD-Runge-Kutta scheme from [7] for the time integration did not yield a third order accurate scheme in total for $q > 2$. Meanwhile, in [5], our results of [12] have been extended to the case of nonuniform meshes (for $\varepsilon(h) = h$ and $\varepsilon(h) = h^2$), where the dependency of ε on h is substantial. The remaining question is the explanation of the observed order reduction in the case $q > 2$ and it is the aim of this follow-up paper to explain this observation with further analytical and numerical results.

2 Numerical Scheme

We begin with a brief description of the considered discretization scheme. The underlying CTO-WENO reconstruction procedure is described for the scalar case in Sect. 2.1, and also the new results in Sect. 3 refer to the scalar case. Nevertheless, the fully discrete scheme in Sect. 2.2 is given for the system case.

2.1 Reconstruction Procedure

The CTO-WENO reconstruction procedure from [14] based on cell averages builds a core part of the analysed scheme. As in [12] we consider $u = u(x)$ as function of the spatial variable only since the procedure is independent of the time variable. Further, we assume a uniform grid with spatial grid size h, grid points $x_j = x_0 + jh$ and corresponding finite volumes $I_j = [x_j - \frac{h}{2}, x_j + \frac{h}{2}] = [x_{j-\frac{1}{2}}, x_{j+\frac{1}{2}}]$. The task is to reconstruct the function u by a piecewise polynomial approximation P given the

cell averages over all I_j,

$$\bar{u}_j = \frac{1}{h} \int_{x_{j-\frac{1}{2}}}^{x_{j+\frac{1}{2}}} u(x)dx\,.$$

For this, we will use (in each cell I_j) a convex combination of three polynomials P_{L}, P_{C} and P_{R},

$$P(x) = w_{\mathrm{L}}P_{\mathrm{L}}(x) + w_{\mathrm{C}}P_{\mathrm{C}}(x) + w_{\mathrm{R}}P_{\mathrm{R}}(x) \tag{2}$$

with $w_i \geq 0$ for all $i \in \{\mathrm{L}, \mathrm{C}, \mathrm{R}\}$ and $w_{\mathrm{L}} + w_{\mathrm{C}} + w_{\mathrm{R}} = 1$. To improve the readability, we leave out the index j indicating the considered interval for the polynomials and other terms, wherever it is clear from the context.

The polynomials P_{L} and P_{R} are one-sided linear reconstructions,

$$P_{\mathrm{L}}(x) = \bar{u}_j + \frac{\bar{u}_j - \bar{u}_{j-1}}{h}(x - x_j)\,, \qquad P_{\mathrm{R}}(x) = \bar{u}_j + \frac{\bar{u}_{j+1} - \bar{u}_j}{h}(x - x_j)\,.$$

For the third polynomial P_{C} we need the parabola P_{opt}, which is the unique parabola that conserves the three cell averages $\bar{u}_{j-1}$, $\bar{u}_j$, $\bar{u}_{j+1}$. Then, for given (positive) constants c_{L}, c_{R} and $c_{\mathrm{C}} = 1 - c_{\mathrm{L}} - c_{\mathrm{R}}$, P_{C} is chosen in such a way that

$$P_{\mathrm{opt}}(x) = c_{\mathrm{L}}P_{\mathrm{L}}(x) + c_{\mathrm{C}}P_{\mathrm{C}}(x) + c_{\mathrm{R}}P_{\mathrm{R}}(x) \tag{3}$$

holds. For the weights in (2) we use

$$w_i = \frac{\alpha_i}{\sum_k \alpha_k}\,, \quad \text{where} \quad \alpha_i = \frac{c_i}{(\varepsilon(h) + IS_i)^p} \quad i, k \in \{\mathrm{L}, \mathrm{C}, \mathrm{R}\} \tag{4}$$

and the smoothness indicators

$$IS_i = \sum_{k=1}^{2} \int_{x_{j-\frac{1}{2}}}^{x_{j+\frac{1}{2}}} h^{2k-1}\left(P_i^{(k)}(x)\right)^2 dx \qquad i \in \{\mathrm{L}, \mathrm{C}, \mathrm{R}\}\,. \tag{5}$$

In (4) we apply $\varepsilon(h) = Kh^q$ (with $K = 1$ in all examples) and usually $p = 2$. For the constants c_i in (3) and (4), we use $c_{\mathrm{L}} = c_{\mathrm{R}} = 0.25$ as in [14] and accordingly $c_{\mathrm{C}} = 1 - c_{\mathrm{L}} - c_{\mathrm{R}} = 0.5$.

2.2 Fully Discrete Scheme

We now give a brief description of a complete numerical scheme to solve (1) based on the CTO-WENO reconstruction procedure presented in Sect. 2.1 (cf. [12, 13]). Note that the whole scheme can be applied to systems of conservation laws, where the reconstruction procedure can for instance be applied componentwise. First, for a given mesh size h, we average (1) over all intervals I_j. This yields the initial conditions

$$\bar{u}_j(0) = \frac{1}{h} \int_{x_{j-\frac{1}{2}}}^{x_{j+\frac{1}{2}}} u_0(x)dx \tag{6}$$

for the cell averages in each interval I_j, and the evolution equation

$$\frac{d}{dt}\bar{u}_j(t) = -\frac{1}{h}\big(f(u(x_{j+\frac{1}{2}},t)) - f(u(x_{j-\frac{1}{2}},t))\big)\,. \tag{7}$$

Next, the fluxes $f(u(x_{j\pm\frac{1}{2}},t))$ at the cell boundaries are replaced/approximated by a numerical flux $H_{j\pm\frac{1}{2}}(t)$ – here, corresponding to the central scheme in [13], by the local Lax-Friedrichs flux

$$H_{j+\frac{1}{2}}(t) = \frac{f(u^+_{j+\frac{1}{2}}(t)) + f(u^-_{j+\frac{1}{2}}(t))}{2} - \frac{a_{j+\frac{1}{2}}(t)}{2}\big(u^+_{j+\frac{1}{2}}(t) - u^-_{j+\frac{1}{2}}(t)\big) \tag{8}$$

with

$$a_{j+\frac{1}{2}}(t) = \max_{u\in C(u^-_{j+\frac{1}{2}}(t),u^+_{j+\frac{1}{2}}(t))} \rho\left(\frac{\partial f}{\partial u}(u)\right) \tag{9}$$

and

$$u^-_{j+\frac{1}{2}}(t) = P_j(x_{j+\frac{1}{2}},t) \qquad \text{and} \qquad u^+_{j+\frac{1}{2}}(t) = P_{j+1}(x_{j+\frac{1}{2}},t)\,.$$

The polynomials P_j and P_{j+1} are reconstructed from the cell averages at time t according to the procedure described in Sect. 2.1. Further, $\rho(A)$ denotes the spectral radius of the matrix A and $C(u^-_{j+\frac{1}{2}}(t), u^+_{j+\frac{1}{2}}(t))$ is the curve in the phase space that connects $u^-_{j+\frac{1}{2}}(t)$ and $u^+_{j+\frac{1}{2}}(t)$ via a Riemann fan.

Finally, the third order TVD Runge-Kutta scheme of [7] is used for the time integration of the semi-discretized problem

$$\frac{d}{dt}\bar{u}_j^h(t) = -\frac{1}{h}\big(H_{j+\frac{1}{2}}(t) - H_{j-\frac{1}{2}}(t)\big)$$

with approximate solution $\bar{u}^h$ and initial conditions from (6).

3 New Results

3.1 A Sufficient Condition in the Linear Case

A usual argumentation for an mth order scheme (with respect to the spatial semi-discretization) goes as follows: The exact evolution of the cell averages in each interval I_j is given by (7). Now assume that the numerical flux satisfies

$$H_{j+\frac{1}{2}}(t) = f(u(x_{j+\frac{1}{2}}, t)) + d(x_{j+\frac{1}{2}}, t)\, h^m + \mathcal{O}(h^{m+1}) \tag{10}$$

with a Lipschitz continuous function $d(x, t)$ with Lipschitz constant L_d (with respect to x). Then,

$$\frac{H_{j+\frac{1}{2}}(t) - H_{j-\frac{1}{2}}(t)}{h} = \frac{f(u(x_{j+\frac{1}{2}}, t)) - f(u(x_{j-\frac{1}{2}}, t))}{h} + \Big(\underbrace{d(x_{j+\frac{1}{2}}, t) - d(x_{j-\frac{1}{2}}, t)}_{\|\ldots\| \le L_d h}\Big) h^{m-1} + \mathcal{O}(h^m)$$

and further (as desired)

$$\frac{d}{dt}\bar{u}_j(t) = -\frac{1}{h}\big(H_{j+\frac{1}{2}}(t) - H_{j-\frac{1}{2}}(t)\big) + \mathcal{O}(h^m)\,.$$

In the simplest case of a linear flux function, $f(u) = au$ with $a > 0$ (w.l.o.g.), the local Lax-Friedrichs flux (8) reduces to $H_{j+\frac{1}{2}}(t) = a u^-_{j+\frac{1}{2}}(t)$ and the "sufficient condition" (10) directly reduces to an accuracy condition

$$u^-_{j+\frac{1}{2}}(t) - u(x_{j+\frac{1}{2}}, t) = \tilde{d}(x_{j+\frac{1}{2}}, t)\, h^m + \mathcal{O}(h^{m+1}) \tag{11}$$

with a Lipschitz continuous function $\tilde{d}(x, t) = d(x, t)/a$ (with respect to x). Further, since $u^-_{j+\frac{1}{2}}(t) = P_j(x_{j+\frac{1}{2}}, t)$, we have to take a closer look at the accuracy of the reconstruction polynomials P_j given by (2). Actually, we are interested in the case

$m = 3$ (a third order scheme in the smooth case). From the proof of Theorem 2.1 in [12], we see that the deviation

$$c_i - w_i = \mathcal{O}(h)$$

from the optimal weights is essential to get third order accuracy in the reconstruction since this deviation is multiplied with the interpolation error of the single polynomials P_i, which is at least $\mathcal{O}(h^2)$ (in the smooth case). To also fulfill (11), it would be sufficient to have

$$c_i - w_i = d_i(x_j, t)\, h + \mathcal{O}(h^2) \tag{12}$$

with Lipschitz continuous functions d_i.

3.2 *Failure of $q > 2$: Numerical Evidence*

According to the sufficient condition (12), it should be revealing to look at $\frac{c_i - w_i}{h}$ for $h \to 0$. Therefore, we consider the initial conditions of the first "failing" example of [12] (originally from [10]),

$$u_0(x) = \sin\left(\pi x - \sin(\pi x)/\pi\right)$$

on the computational domain $x \in [-1, 1]$ (with periodic boundary conditions). For $Nx = 2^n$ grid cells with $n \in \{10, 15, 20\}$, corresponding to $h = 2 \cdot 2^{-n}$, we apply the CTO-WENO reconstruction with $\varepsilon(h) = h^3$ and evaluate $\frac{c_i - w_i}{h}$ for each cell and $i \in \{\text{L}, \text{C}, \text{R}\}$.

Figure 1 shows the corresponding results. Note the different scales on the y-axes and the different behaviour for $i \in \{\text{L}, \text{R}\}$ in comparison to $i = \text{C}$. Obviously, the quotient $\frac{c_i - w_i}{h}$ seems to be unbounded at least for $i \in \{\text{L}, \text{R}\}$ and $h \to 0$ close to the zeros of u_0' (at approximately ± 0.597). At the first view, this observation even seems to be contradictory to the results of [12], but the quotient is bounded for each fixed position x_j so that finally $w_i = c_i + \mathcal{O}(h)$ holds for arbitrary x also in the considered case $\varepsilon(h) = h^3$. Nevertheless, this behaviour is much different from the results one observes in the case $\varepsilon(h) = h^q$ with $q \leq 2$ and it obstructs the "sufficient condition" (12).

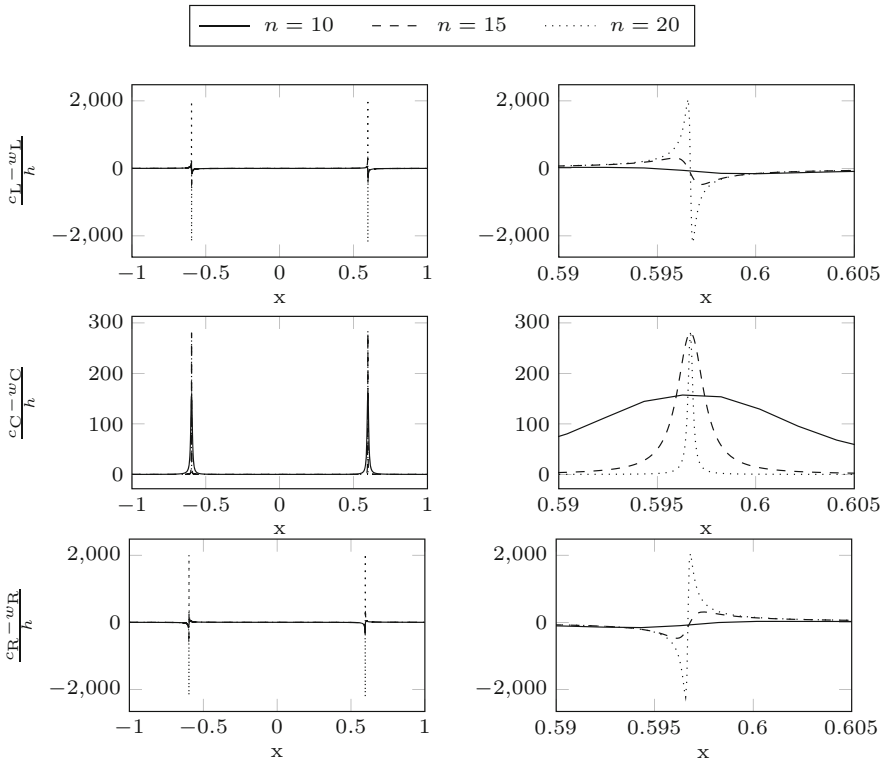

Fig. 1 Differences $\frac{c_i - w_i}{h}$ for $i \in \{\text{L}, \text{C}, \text{R}\}$, $h = 2 \cdot 2^{-n}$ with $n \in \{10, 15, 20\}$, $\varepsilon(h) = h^3$. The plots in the *right column* are zoomed from the plots in the *left column*

3.3 Failure of $q > 2$: Analytical Evidence

Next, we aim to explain the observation above from the analytical point of view. First, the proof of Theorem 3.3 in [12] gives us for any fixed x_j

$$c_i - w_i = -p f_i h^r + \mathcal{O}(h^{r+1})$$

with $r \geq 1$ and $f_i = -\sum_k c_k e_{ik}$, where the e_{ik} are given by

$$\frac{IS_i - IS_k}{\varepsilon(h) + IS_k} = e_{ik} h^r + \mathcal{O}(h^{r+1}) .$$

The term on the left-hand side can be expressed as

$$\frac{IS_i - IS_k}{\varepsilon(h) + IS_k} = \frac{c_{ik}h^{2s+2} + d_{ik}h^{2s+3} + \mathcal{O}(h^{2s+4})}{Kh^q + a_k h^{2s+2} + b_k h^{2s+3} + \mathcal{O}(h^{2s+4})} \tag{13}$$

with $s = s_j$ (multiplicity of the zero of u' at x_j, or 0 if $u'(x_j) \neq 0$) and appropriate constants a_i and b_i, $c_{ik} = a_i - a_k$ and $d_{ik} = b_i - b_k$ from

$$IS_i = a_i h^{2s+2} + b_i h^{2s+3} + \mathcal{O}(h^{2s+4})$$

and

$$IS_i - IS_k = c_{ik}h^{2s+2} + d_{ik}h^{2s+3} + \mathcal{O}(h^{2s+4}) .$$

Motivated by the numerical results above, we take a closer look at the zeros of u'. Considering $s_j > 0$ for $q \in (2, 3]$ gives

$$\frac{IS_i - IS_k}{\varepsilon(h) + IS_k} = \frac{d_{ik}h^{2s+3-q} + \mathcal{O}(h^{2s+4-q})}{K + a_k h^{2s+2-q} + \mathcal{O}(h^{2s+3-q})} = \frac{d_{ik}}{K}h^{2s+3-q} + \mathcal{O}(h^{2s+4-q}) ,$$

for even s_j (where $c_{ik} = 0$ according to [12]), and for odd s_j

$$\frac{IS_i - IS_k}{\varepsilon(h) + IS_k} = \frac{c_{ik}h^{2s+2-q} + \mathcal{O}(h^{2s+3-q})}{K + a_k h^{2s+2-q} + \mathcal{O}(h^{2s+3-q})} = \frac{c_{ik}}{K}h^{2s+2-q} + \mathcal{O}(h^{2s+3-q}) .$$

Due to the dominant role of the constant K in the denominator (and $2s + 2 - q \geq 1$), this case seems to be uncritical. The real problem are the points close to the zeros of u': In the case $s_j = 0$, we get for $q \in (2, 3]$

$$\frac{IS_i - IS_k}{\varepsilon(h) + IS_k} = \frac{d_{ik}h + \mathcal{O}(h^2)}{Kh^{q-2} + a_k + b_k h + \mathcal{O}(h^2)} = \frac{d_{ik}}{a_k}h + \mathcal{O}(h^{q-1}) , \tag{14}$$

where again $c_{ik} = 0$ according to [12]. From the proof of Lemma 3.1 in [12], we know that $a_k = \left(u'(x_j)\right)^2$ here, whereas b_k and therewith d_{ik} are proportional to $u'(x_j)u''(x_j)$. For any fixed x_j with $u'(x_j) \neq 0$, Eq. (14) is sufficient to finally get third order accuracy for the CTO-WENO reconstruction, but obviously the factor $e_{ik} = \frac{d_{ik}}{a_k}$, which is proportional to $u''(x_j)/u'(x_j)$, is not bounded uniformly in x close to zeros of u' (unless also u'' vanishes in that point). This clearly explains the increase of the quotient $\frac{c_i - w_i}{h}$ for $h \to 0$ close to the zeros of u' and therewith finally leads to the observed order reduction.

Remark 1 Obviously, for $q \leq 2$ the term $\varepsilon(h) = Kh^q$ is always part of the dominant term in the denominator of (13) (as already noted in [12]) and therefore the quotient $\frac{c_i - w_i}{h}$ stays bounded in that case and even the sufficient condition (12) is fulfilled.

Remark 2 Reconsidering the scalar accuracy tests from [12], one actually observes that third order accuracy is achieved by the fully discrete scheme with $\varepsilon(h) = h^3$ apart from critical points.

4 Conclusion

The aim of this work was to explain the order reduction one observes for a fully discrete scheme based on the CTO-WENO reconstruction procedure with $\varepsilon(h) = Kh^q$ with $q \in (2, 3]$, whereas the pure spatial reconstruction is (pointwise) third order accurate. Therefore, we took a closer look at the error expansions and found numerical as well as analytical evidence for the "failure" of this parameter range. Consequently, at least for the usual choice $p = 2$ in the weight design, the region of practical interest is $q \in [1, 2]$, for which meanwhile third order accuracy has also been shown for the case of nonuniform meshes in [5].

References

1. F. Aràndiga, A. Baeza, A.M. Belda, P. Mulet, Analysis of WENO schemes for full and global accuracy. SIAM J. Numer. Anal. **49**(2), 893–915 (2011)
2. R. Borges, M. Carmona, B. Costa, W.S. Don, An improved weighted essentially non-oscillatory scheme for hyperbolic conservation laws. J. Comput. Phys. **227**(6), 3191–3211 (2008)
3. S. Bryson, D. Levy, Mapped WENO and weighted power ENO reconstructions in semi-discrete central schemes for Hamilton-Jacobi equations. Appl. Numer. Math. **56**(9), 1211–1224 (2006)
4. M. Castro, B. Costa, W.S. Don, High order weighted essentially non-oscillatory WENO-Z schemes for hyperbolic conservation laws. J. Comput. Phys. **230**(5), 1766–1792 (2011)
5. I. Cravero, M. Semplice, On the accuracy of WENO and CWENO reconstructions of third order on nonuniform meshes. J. Sci. Comput. **67**(3), 1219–1246 (2016)
6. H. Feng, F. Hu, R. Wang, A new mapped weighted essentially non-oscillatory scheme. J. Sci. Comput. **51**(2), 449–473 (2012)
7. S. Gottlieb, C.-W. Shu, Total variation diminishing Runge-Kutta schemes. Math. Comput. **67**, 73–85 (1998)
8. Y. Ha, C.H. Kim, Y.J. Lee, J. Yoon, An improved weighted essentially non-oscillatory scheme with a new smoothness indicator. J. Comput. Phys. **232**(1), 68–86 (2013)
9. A. Harten, B. Engquist, S. Osher, S.R. Chakravarthy, Uniformly high order accurate essentially non-oscillatory schemes, III. J. Comput. Phys. **71**(1), 231–303 (1987)
10. A.K. Henrick, T.D. Aslam, J.M. Powers, Mapped weighted essentially non-oscillatory schemes: achieving optimal order near critical points. J. Comput. Phys. **207**(2), 542–567 (2005)
11. G.-S. Jiang, C.-W. Shu, Efficient implementation of weighted ENO schemes. J. Comput. Phys. **126**(1), 202–228 (1996)
12. O. Kolb, On the full and global accuracy of a compact third order WENO scheme. SIAM J. Numer. Anal. **52**(5), 2335–2355 (2014)
13. A. Kurganov, D. Levy, A third-order semidiscrete central scheme for conservation laws and convection-diffusion equations. SIAM J. Sci. Comput. **22**(4), 1461–1488 (2000)
14. D. Levy, G. Puppo, G. Russo, Compact central WENO schemes for multidimensional conservation laws. SIAM J. Sci. Comput. **22**(2), 656–672 (2000)

15. X.-D. Liu, S. Osher, T. Chan, Weighted essentially non-oscillatory schemes. J. Comput. Phys. **115**(1), 200–212 (1994)
16. S. Serna, A. Marquina, Power ENO methods: a fifth-order accurate weighted power ENO method. J. Comput. Phys. **194**(2), 632–658 (2004)
17. N.K. Yamaleev, M.H. Carpenter, A systematic methodology for constructing high-order energy stable WENO schemes. J. Comput. Phys. **228**(11), 4248–4272 (2009)
18. N.K. Yamaleev, M.H. Carpenter, Third-order energy stable WENO scheme. J. Comput. Phys. **228**(8), 3025–3047 (2009)